Experimental characterization of isothermal and evaporative sprays

Y. Hardalupas*, S. Sahu and AMKP Taylor
Department of Mechanical Engineering
Imperial College London
London, SW7 2AZ, UK

Abstract

This paper demonstrates the potential of two novel experimental approaches to characterize isothermal and evaporative sprays respectively. Both approaches use the out-of-focus imaging technique 'Interferometric Laser Imaging Droplet Sizing' (ILIDS) for planar simultaneous droplet size and velocity measurements. The study of the isothermal spray aims at characterizing the interaction between the dispersed and continuous phase, which requires simultaneous measurement of the gas velocity in the vicinity of individual droplets. For this purpose, ILIDS is combined with 'Particle Image Velocimetry' (PIV). The combined measurements are presented in a model co-flowing isothermal spray dryer with a spray injected from a single air-assist solid cone atomizer. The measurements were obtained at 500 mm downstream from the atomiser, at 125 mm off-axis location in the spray and at five different cross-stream locations, situated at 0, 50, 100, 150 and 185mm respectively from the spray axis. The results include the mean droplet velocity and the rms of the velocity fluctuations for three representative size classes of the spray with corresponding Stokes numbers less than unity, the mean velocity and the rms of the velocity fluctuations of the gas flow, and the spatial correlations of the gas and droplet velocity fluctuations, conditional on droplet size class. The spatial correlation coefficients of droplet-gas velocity fluctuations for different size classes were compared with those of the droplet-droplet and gas-gas velocity fluctuations for various cross-stream locations. The selective influence of the large scale eddy structures of the gas phase flow, extracted through Proper orthogonal decomposition (POD), on the droplet-gas flow interaction was examined. For evaporative sprays, the aim is to understand the interaction between droplet evaporation and mixing process and assess its importance on combustion. In order to accomplish this, ILIDS, for measurement of droplet characteristics, is combined with 'Laser Induced fluorescence' (LIF) for the measurement of vapour concentration. The experimental arrangement for the combined ILIDS and LIF technique is described and preliminary results are obtained in mono-sized droplet streams for two droplet sizes. The optical arrangement, which combines an out-of-focus with a focused optical technique, causes a discrepancy between the centres of the same droplet at the focused and defocused images. This discrepancy is theoretically evaluated for imaging through the combined ILIDS and LIF techniques and compared with the corresponding discrepancy for the combined ILIDS and PIV techniques.

Introduction

In liquid-fuelled combustion, the formation and combustion of air-fuel mixture are mostly influenced by the interaction between droplets and entrained fluid flow, droplet cluster formation [1] and group combustion [2]. But, the complex spray combustion involves different interacting processes such as chemistry, heat transfer, turbulent two-phase flow dynamics, and evaporation and mixing. The combination of all these processes makes the understanding of the physics challenging. Hence, there is a need to investigate these processes separately and the present paper focuses on the study of spatial and temporal variations in the spray characteristics of a steady spray under isothermal and evaporative conditions respectively. Therefore, the paper studies (a) the interaction between the droplet characteristics and the continuous gas phase flow in an isothermal spray and (b) the influence of droplet characteristics on the vapour phase in evaporating sprays.

The first aim is to report the measurement of droplet-gas spatial velocity correlations in an isothermal spray. For a droplet-laden gas flow, the turbulent kinetic energy equation for the continuous phase contains terms, which include correlations of droplet concentration and velocity fluctuations of the fluid and/or droplets and droplet-fluid velocity correlations. They represent an 'extra' source or sink of turbulent kinetic energy in the fluid and depict the interaction [3, 4]. The feasibility of incorporation of the effect of two-way coupling (*i.e* modification of turbulence by droplets through interfacial momentum transfer) depends on successful modelling of these cross-correlation terms. Also, several important issues, usually absent in numerical models, including turbulence generation due to wakes from droplets, effect of gravity and the presence of distribution of droplet sizes, should be considered. Thus, experimental characterization of the droplet-gas flow interaction in sprays is important for the understanding of the underlying mechanisms and the provision of appropriate data that can

* Corresponding author: y.hardalupas@imperial.ac.uk

assist the development and evaluation of computational models. However, only few experimental studies have been reported in this regard [e.g. 3 - 7] due to difficulties to obtain such measurements. The measurement difficulty arises from two challenging factors: first, the estimation of the above mentioned correlation terms require simultaneous *planar* measurement of velocity of both phases, and secondly, the correlations have to be calculated *conditional* on droplet size-classes. However, the literature, till date, is restricted to single-point measurements and/or mono-sized droplet/particle consideration. Thus, there is a need of experimental characterization of, not only the relative velocity between droplets and gas phase and associated spatial correlations of velocity fluctuations, but also the measurement of droplet size simultaneously, which is the first aim of the present research. A new approach of simultaneous planar measurement of droplet velocity and size with gas phase velocities is adapted for this purpose, based on a combination of the out-of-focus imaging technique 'Interferometric Laser Imaging Droplet Sizing' (ILIDS) [8, 9] for planar simultaneous droplet size and velocity measurements with the in-focus technique 'Particle Image Velocimetry' (PIV) for gas flow velocity measurements in the vicinity of individual droplets. The advantage of the present approach lies in the fact that the position of droplets in a spray, obtained by ILIDS beforehand, helps in identifying the images of the same droplets (as glare-points) in the focused PIV image, thus making it possible to associate the droplet size to the glare-points. The glare-points from the PIV image are removed retaining only 'seeding' particles, which follow the gas phase flow. The PIV images are then processed to obtain the gas velocity in the vicinity of each droplet. An unexpected difficulty with the combined technique was the presence of a discrepancy in droplet centre when calculated independently through ILIDS and PIV images, which would lead to erroneous association of droplet size in the focused PIV images. The cause of this discrepancy, its quantification and a method for its elimination were addressed in [10, 11]. The objectives of the paper here are to present two phase measurements with the combined ILIDS and PIV techniques in a low Stokes number, polydispersed spray region of a model spray dryer at various cross-stream locations. The results include the mean and rms of velocity fluctuations of the two phases, the spatial droplet-droplet and droplet-gas velocity correlations conditional on droplet size classes for different cross-stream locations and comparison between them. Proper Orthogonal Decomposition (POD) was applied to the instantaneous gas flow velocity to extract the large-scale eddy structures (eigen-modes) of the continuous phase. The contribution of individual POD modes on the spatial correlation of the droplet-gas velocity fluctuations was quantified by reconstructing the instantaneous gas velocity field associated with each mode and recalculating the spatial correlations of the resulting gas flow with different droplet size classes.

The second aim is to understand the interaction between droplet characteristics and evaporation process in evaporating sprays and assess its importance on mixing and combustion. An evaporating spray and its interaction with the surrounding gas are considered. This necessitates development of an optical technique, which can correlate the vapour concentration around droplets with the droplet characteristics, like drop size, velocity and concentration, and can elucidate on the conditions under which group evaporation [2] occurs and identify the range of associated group evaporation numbers in an evaporative spray. Therefore, the technique should be capable of providing simultaneous and planar measurements of vapour concentration and droplet size, velocity and concentration. Therefore, the current paper presents the potential of an approach, which combines ILIDS for planar measurement of droplet properties with 'Laser Induced Fluorescence' (LIF) for vapour concentration distribution. Measurements with the combined approach are demonstrated in a mono-sized droplet stream operating with two droplet sizes.

The paper describes the associated experimental arrangements, addresses the issue of the discrepancy in droplet centre between focused and defocused techniques and presents results from the two novel measurement approaches applied in isothermal and evaporating sprays. The paper ends with a discussion and a summary of the main findings.

Experimental setup for the combined ILIDS with PIV and ILIDS with LIF measurements

The fundamental principle of combining the optical arrangements of ILIDS with PIV techniques and the experimental set-up are described in detail in [10, 11]. A brief summary is presented here. As shown in Fig. 1a, the reflected and first order refracted light scattered from the droplet, interfere to produce parallel fringes on a defocused plane [8] and the characteristic interferogram is observed with a far field arrangement of receiving optics [9] through camera 1 (Fig. 1a). The number of fringes present in each of the imaged fringe patterns and the fringe spacing is proportional to the diameter. For the purpose of characterizing simultaneously the velocity of the air flow in the vicinity of individual droplets, the air surrounding the spray must be seeded with fine tracer particles and the viewing area is imaged on the focal plane for PIV measurements. This is achieved by splitting a part of the incoming scattered light using a beam splitter and collecting it through a second camera (camera 2) placed at the focal plane (Fig. 1a). With this optical system, bright spots called glare points, corresponding to focused reflected and refracted rays, appear on the image recorded by camera 2. Hence, the same droplet is imaged as a rectangular region with a superimposed fringe pattern on the ILIDS camera and as distribution of two glare points on the PIV image. The defocused images from 'seeding' tracer particles appear on the ILIDS camera, but without any superimposed fringes. The droplet positions obtained through ILIDS can be used to detect

their corresponding glare points in the PIV image. In this way, the detected glare points can be removed from the PIV image and the filtered PIV image, when processed, provides gas velocity around each droplet.

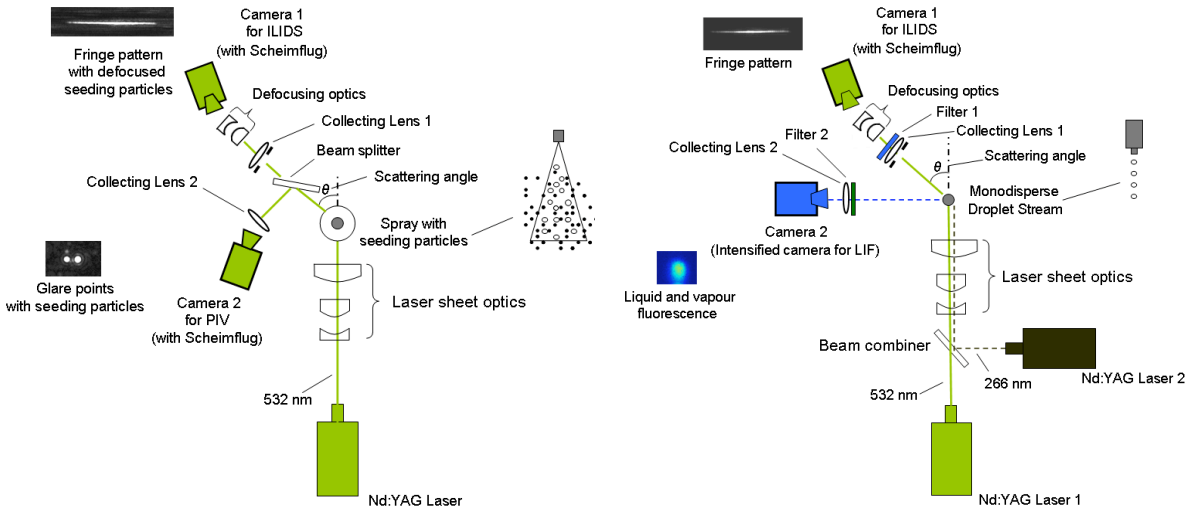

Figure 1: Optical arrangement for (a) combined ILIDS and PIV techniques; (b) combined ILIDS and LIF techniques.

The present work employed a spray dryer rig for the combined ILIDS/PIV measurements [10, 11]. The rig allowed coflowing air to enter from the top in the annulus around the atomizer, which was a custom–built air–assisted nozzle placed on the centerline of the cylindrical chamber with diameter of 0.5m. It produced a solid cone water spray with a characteristic droplet diameter (SMD) of the order of 150–200 µm at liquid feed rates of the order of $1.4\text{-}1.6\times10^{-3}$ kg/s and air feed rate of the order of 0.12×10^{-3} kg/s. The coflowing air was seeded with aluminium oxide particles (diameter range 1-5 micron) before entering the rig. The coflowing air flowrate, carrying the seeding particles, was 200 lt/min, resulting in area-averaged air velocity 1.7×10^{-2}m/s around the spray. A frequency-doubled, double pulse Nd:YAG laser (120 mJ/pulse at 532 nm; New Wave Research) was used to illuminate the flow. The thickness of the laser sheet was about 1mm. Two identical cameras were used (PCO; Sensicam QE, 12bit, 1040×1376) and positioned on the same side of the laser sheet. Two identical lenses (Nikon; 135mm focal length) were used to collect the scattered light from droplets. The scattered light from droplets was divided into two parts by using a beam splitter. Because of issues related to optical aberrations of ILIDS images, both cameras were adjusted to provide a field of view of approximately 8×12 mm^2. The resolution was approximately 9µm/pixel in both directions for both cameras. In all experiments, the scattering angle was set at $\theta = 69°$, which is the optimum scattering angle for water droplets for ILIDS droplet sizing with a vertically polarized laser sheet. The collecting angle of the lens was set to 5.09°, resulting in a resolution of 6.59 [µm/fringe] for the ILIDS system. Both cameras were aligned under the Scheimpflug condition [11], as required for imaging at off-axis scattering angles.

The optical arrangement for the combined ILIDS and LIF measurements is shown in Fig. 1b. For ILIDS droplet sizing, the flow field is illuminated by Nd:YAG Laser 1 at wavelength 532nm. The camera 1 was set at scattering angle $\theta = 70°$, which is the optimum forward scattering for acetone droplets for ILIDS operation with vertically polarized light, and Scheimpflug condition was maintained. The laser and camera specifications were the same as for the combined ILIDS/PIV technique. For LIF measurement, acetone was selected as a fluorescence marker because of its low dependence on temperature. Acetone droplets absorb the UV light when excited by the fourth harmonic generator Nd:YAG Laser 2 (120 mJ/pulse at 266 nm; Continuum Lasers) and fluoresce in the blue range (350 - 550 nm with peak around 435nm), which is independent of the phase of the molecules. Both scattered and fluorescent intensities were collected through two identical lenses (Nikon; 100mm focal length). The lenses, being made of BK7, could absorb the scattered UV light at 266nm. The fluorescent intensity was collected through camera 2 (Fig. 1b), a gated intensified CCD camera (IRO image intensifier with PCO; Sensicam QE, 12bit, 1040×1376). Because of experimental constraints, the Scheimpflug condition could not be incorporated in camera 2 which did not allow placing the camera at the same scattering angle θ as camera 1, and similar to the ILIDS/PIV system. Thus, camera 2 was placed at a right angle to the laser sheet. The acetone droplets scatter light at 532nm without absorbing. The wavelengths of the scattered and fluorescent intensities, being almost distinct from each other, allowed separating the required signal before each camera with suitable optical filters. For quantitative measurement of vapour concentration, the fluorescent intensity of the LIF images must be calibrated with respect to a known concentration. The calibration was performed under the same optical arrangement. Air is allowed to enter into liquid acetone present in a container with initially known volume. The

captured LIF images corresponded to the air, coming out of the container, almost saturated with acetone. For a given time interval, the vapour concentration could be calculated from the known volume of air and vaporised liquid acetone. Thus, the calibration curve of fluorescent intensity versus acetone vapour concentration could be obtained for various air flow rates.

Droplet centre discrepancy

It might be expected that the centre of any given droplet in the two images, obtained from ILIDS and either from PIV or LIF, should coincide within the experimental error of registration. However, this is not correct. This problem of droplet centre discrepancy has been rarely recognized in the literature. One exception is [12], who, while describing the method of combining ILIDS with laser-induced fluorescence (LIF) for simultaneous vapour concentration measurement along with droplet properties, noticed the discrepancy of droplet position in the two images. The reason behind the occurrence of the droplet positioning error was attributed to "the accuracy of position calibration caused by the use of two cameras for each measurement''. However, as discussed in [10, 11], for the combined ILIDS with PIV technique, straightforward combination of the two optical arrangements results in a discrepancy in the location of the centre of a droplet, when imaging through each technique, which may lead to erroneous identification of the glare points from droplets on the PIV images. The magnitude of the discrepancy was found to be a function of position of the droplet image on the CCD array and the degree of defocus, but almost independent of droplet size. Specifically, it varies approximately linearly across the image along the direction of propagation of the laser sheet for a given defocus setting in ILIDS. The evaluated error from the measurements with monodispersed droplets was subtracted from the droplet centre identified in ILIDS images from a polydispersed spray without 'seeding' particles. This reduced the discrepancy between PIV and ILIDS droplet centres from about 1000 micron to about 100 micron and hence increased the probability of finding corresponding fringe patterns on the ILIDS image and glare points on the PIV image. References [10, 11] also reported a theoretical analysis, which was based on geometrical optics for a simple optical configuration that replicates the essential features of the optical system. The experimental finding was well supported by the theoretical analysis.

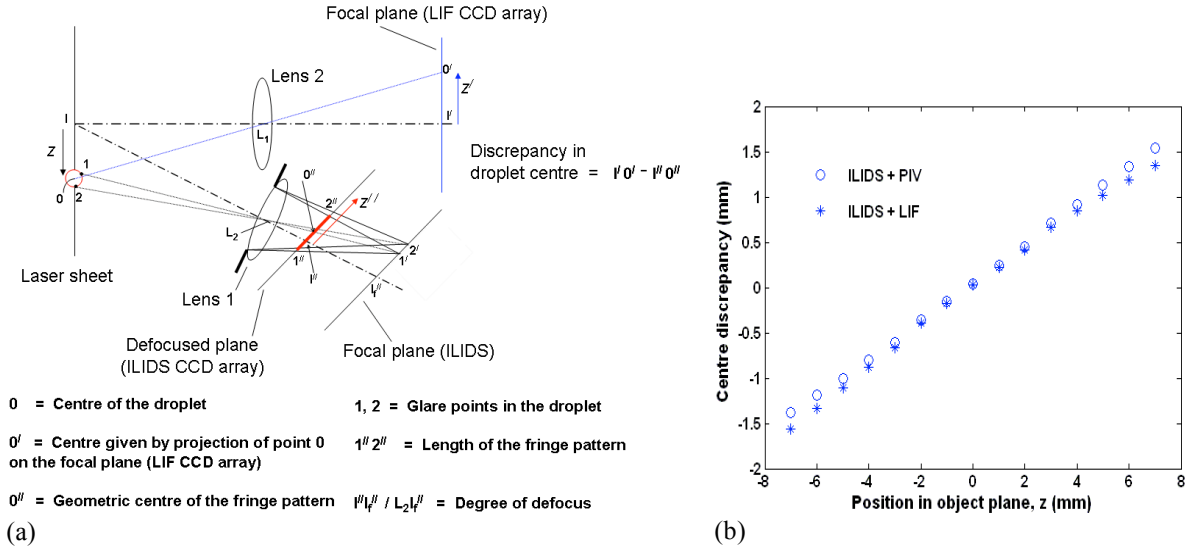

Figure 2: (a) Schematic of the optical system for theoretical prediction of discrepancy in droplet centres between the focused plane in LIF imaging and defocused plane in ILIDS imaging; (b) Discrepancy in geometric centre of the fringe pattern in the ILIDS defocus plane and centre of the droplet image in the LIF focal plane as a function of the *z* position in the object plane. The discrepancy for the case of combined ILIDS with PIV arrangement is also plotted for comparison.

Following the theoretical analysis of [10, 11] for predicting the discrepancy in droplet centre in the combined ILIDS with PIV technique, a similar analysis is briefly presented here which predicts the centre discrepancy for the combined ILIDS with LIF technique. Figure 2 shows the simplified ray diagram for a droplet which is being simultaneously imaged in LIF and ILIDS CCD arrays. All assumptions of the theoretical analysis, reported by [10, 11], remain valid here as well. However the present analysis differs from the previous case, primarily, in two aspects. First, unlike the focal plane in PIV, the focal plane for LIF is perpendicular to the lens axis. Secondly, the fluorescent signal from the liquid droplet is being imaged on the focal plane instead of glare points. Thus, in the present case, for a given droplet within the laser sheet (with droplet centre '0'), the image of

the droplet centre in the focal plane ($0^{/}$) can be obtained straightaway using lens makers formula unlike the case of ILIDS/PIV arrangement, where the droplet centre in the focal plane is determined by the position of midway between the image of both glare points ($1^{/}$ and $2^{/}$). The calibration of the ILIDS and the LIF CCD arrays is carried out with the ILIDS optics adjusted to be in focus, so the coordinate systems fixed to the focussed ILIDS and LIF CCD arrays, both have their origin on the axis of the lens. After calibration, the ILIDS image is defocused by shifting the image plane towards the lens. The degree of defocus is defined as the ratio of the distance between the centres of defocus plane to in-focus plane ($I^{//}I_f^{//}$) to that of centres of lens to in-focus plane ($L_2I_f^{//}$). The geometrical centre of the ILIDS image is $0^{//}$, the mid-point of the fringe pattern $1^{//}2^{//}$. Thus the discrepancy in the centre of the same droplet being imaged in the LIF and ILIDS CCD arrays is equal to $I^{/}0^{/} - I^{//}0^{//}$. The input parameters for the analysis, similar to the experiment, were: $\theta = 70^{o}$, Droplet diameter = 0.2 mm, object distance of both lenses = 200 mm, focal length of both lenses = 100 mm and aperture size = 20 mm. The centre discrepancy is plotted in Fig. 3 for various z locations at the object plane. For comparison purposes, the centre discrepancy for the combined ILIDS with PIV system (under the same optical condition) is also plotted.

Fig. 2b shows that the behaviour of the centre discrepancy in the present case is almost similar to the ILIDS/PIV arrangement, *i.e.* it varies almost linearly across the image plane, from being negative on one side of the image plane to positive on the other side. For the particular parameters considered here, the maximum discrepancy is towards the edge of the CCD array and can be of the order of 1 mm, or five times greater than even the relatively large droplet diameter considered here. Also it was found to be independent of the droplet size. Thus, in order to correctly assign the vapour concentration distribution around the droplets (from LIF) to the droplet size and velocity (from ILIDS), the discrepancy in the droplet centre has to be accounted for.

Combined ILIDS and PIV measurements

The potential of the combined technique for measurement of the characteristics of both phases in sprays, including estimation of droplet-gas spatial velocity correlation (conditional on droplet size classes), was demonstrated for a given location in the spray in [13]. The image processing procedure followed for the combined ILIDS and PIV techniques can be found in [11]. For the details of the process of calculation of the mean and rms of velocity fluctuations, spatial correlation of the droplet-gas velocity fluctuations for different size classes, the related statistical accuracy, and the method of extracting the large scale eddies by applying POD over the instantaneous gas velocity data, the readers are referred to [14]. The present paper discusses the results of the two phase measurements for various cross-stream locations in the spray.

The combined technique was applied in a polydispersed spray with 'seeded' coflowing air around it. The results of the combined ILIDS and PIV measurements are reported for five different cross-stream locations, 500 mm downstream of the nozzle exit, as presented in Figure 3a. At any given measurement location, the notations 'x' and 'y' refer to the *local* axial and cross-stream directions respectively, both lying in the plane of the laser sheet and the corresponding instantaneous velocities are denoted by '$\widetilde{u}$' and '$\widetilde{v}$'. Throughout the paper, the subscript 'd' and 'g' denote droplet and gas respectively. Similarly the subscript 'm' and 'r' respectively denote *mean* and *rms* velocities, and 'overbar' over any quantity indicates time-averaging. The notation 'z' refers to the direction perpendicular to the laser sheet and is measured from the nozzle axis, and 'R 'refers to the *beginning* of any measurement area, at any cross-stream location, measured from the nozzle axis. Because of the experimental constraints in the set-up, measurement was performed at an off-axial position of 125 mm, along the z direction, in order to maintain the required object distance between the viewing area and the collecting lenses. The measurement area was approximately 8mm × 12mm and the cross-stream measurement locations were located at R = 0, 50, 100, 150 and 185 mm respectively from the nozzle axis. For each measurement location, 1700 image pairs were captured through each of the cameras. The repetition rate of the laser was set to 1 Hz, so that the acquired samples remained statistically independent. The laser pulse delay time (ΔT) was chosen to be 150 μs. The measured droplet size distribution is shown in Figure 3b for the measurement location R = 0 mm. The Arithmetic mean droplet diameter (AMD) and Sauter mean diameter (SMD) at this location were 36.4 μm and 48.5 μm respectively. The size distributions at other measurement locations were more or less the same, so they are not shown here. The calculations of the statistical characteristics of the flow field, including mean droplet velocity, rms of droplet velocity fluctuations and the spatial correlations of velocity fluctuations, were performed over three droplet size classes with overall range of 15μm each. These size classes were 20-35μm, 35-50μm and 50-65μm respectively.

Droplet/gas mean and turbulent velocity

Figure 3c shows vector plots of the droplet mean velocity for droplet size classes of 20-35μm, 35-50μm and 50-65μm, and for the gas flow at various cross-stream measurement locations (R) starting from the spray axis and going towards the outer spray region. The mean velocity of droplets of a given size class and the mean gas velocity, at any measurement location, for both axial and cross-stream velocity components could be observed to be quasi-uniform across the measuring area. The corresponding rms of velocity fluctuations was also found to

follow a similar trend. Both the mean and rms velocities of droplets and gas were found to vary within ±20-30% across the measuring area at any given location. At R = 0, the axial mean velocity was of the order of 0.1 ~ 0.2m/s. Typical statistical uncertainty of both axial and cross-stream mean velocities was of the order of ±0.03m/s. The rms of the velocity fluctuations (u_r and v_r) were calculated and found to be of the order of 0.2 ~ 0.3m/s for selected droplet size classes and for the gas phase. It should be noted that the rms velocity in the axial direction was about an order of magnitude greater than the mean velocity and also, was of the same order as the rms velocity in cross-stream direction. The isotropy (u_r / v_r), being close to 'one' and almost spatially invariant, indicates that the flow field (within the viewing area considered here) is nearly homogeneous and isotropic close to the spray axis.

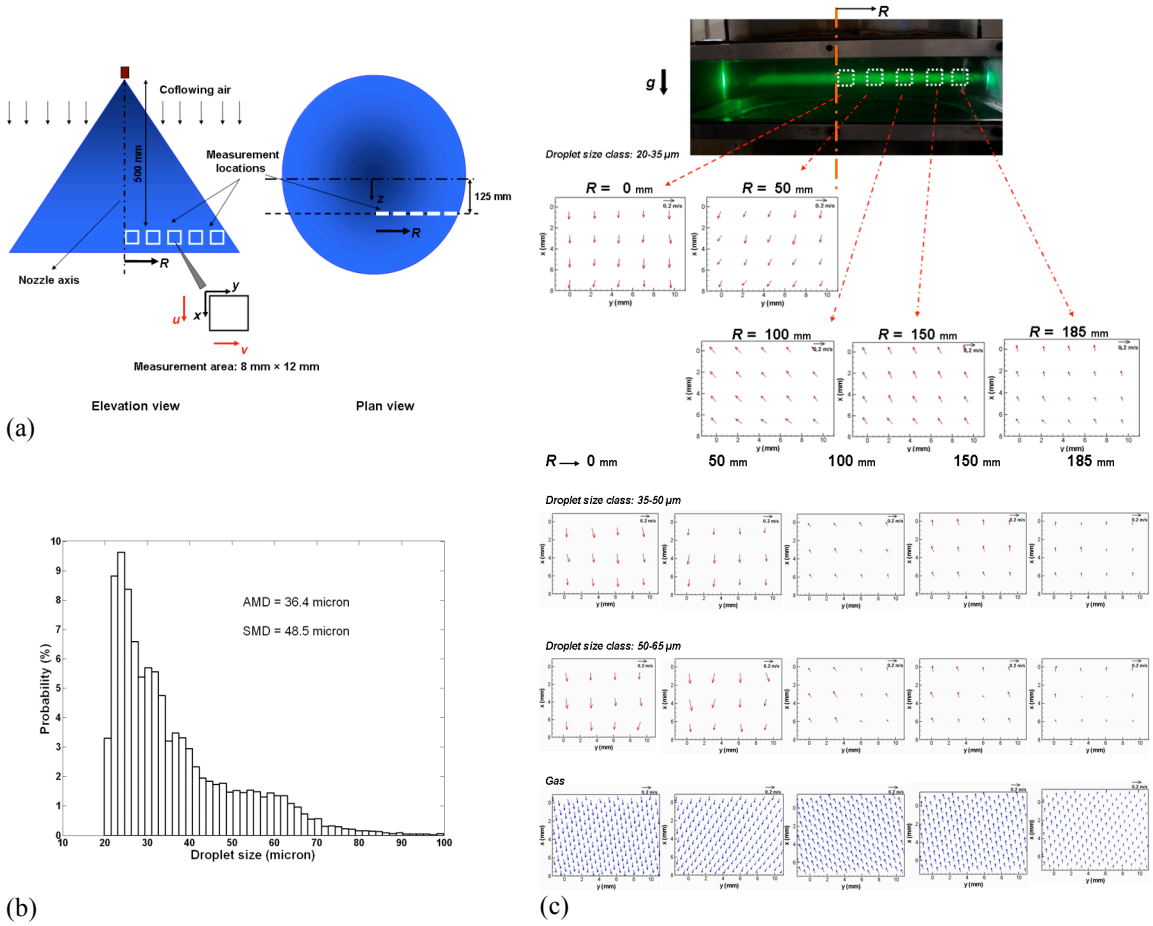

Figure 3: (a) Measurement locations in the spray and the coordinate system. (b) Probability of droplet size in the 8 × 12 mm^2 measurement region at the cross-stream location, R = 0 mm. (c) Mean velocity for droplet size classes of 20-35µm, 35-50µm, and 50-65µm and for the gas flow for various cross-stream measurement locations, R.

The mean velocity of the droplets and gas flow, for all measurement locations (different R) can be compared in Figure 3c. The statistical uncertainty of the mean velocity measurements, at all locations, was of similar order as for the case at R = 0 mm. The mean velocity, at any given location, was approximately independent of droplet size. Though, a small increase or decrease (about 20%) in mean axial velocity of larger droplets (50-65 µm) was observed as compared to the smaller droplet size class 20-35 µm, depending on whether the droplets move downward closer to the spray centre or upward, against gravity, towards the outer region of the spray. The velocity of droplets at the higher size class was found to reduce towards the outer spray region: for instance the axial mean velocity for 50-65 µm droplet size class at R = 185 mm was of the order of 0.06 m/s, one third of the axial velocity at R = 0 mm. The droplets, away from the centre of the spray, tend to move upward, i.e against gravity and "towards the top of the spray tower". This can be interpreted by the motion of the air surrounding the spray being entrained into the spray in a recirculating pattern. The droplets are prevented from drifting downward under the action of gravity, as might be expected, by the upward component of the gas velocity.

Away from the spray axis, the mean axial velocity difference between droplets and gas phase tends to decrease, while the mean cross-stream velocity of the droplets became higher than that of the gas. No significant difference in mean velocity could be observed between droplets and gas at any location R and for all droplet size

classes, resulting in a low value of droplet Reynolds number *Re* (≈ 0.05). Both droplet and gas axial rms velocities were of the same order (similar to the mean velocity) and slightly decreasing away from the spray axis. However, the cross-stream rms velocity for both droplets and gas was found to decrease sharply with *R* (by about 50% from *R* = 0 to *R* = 185 mm), indicating that away from the spray axis, the flow tends to be more anisotropic and the production of turbulent kinetic energy is reduced. The rms velocity for droplets, similar to the mean velocity, was almost independent of droplet size, and the rms velocities for either droplets or gas were an order of magnitude greater than the mean velocity at any given measurement location. Assuming the length scale of the energy containing eddies to be 1/5 of the jet width [15], the integral length scale was estimated to be of the order of 100mm. The Stokes numbers for the 20-35µm, 35-50µm and 20-35µm droplet size classes were of the order of 0.005, 0.015 and 0.025 respectively, based on the integral length scale, which supports good response of droplets to the gas flow velocity fluctuations.

Spatial correlation of droplet and gas velocity fluctuations

The velocity correlation terms were calculated over the whole viewing area for each measurement location, *R*. Since no strong spatial gradients of mean and rms velocity at either axial or cross-stream direction were found within the viewing area, such averaging was expected to have no influence on the magnitude of the correlations. The spatial correlation coefficient between the fluctuating velocity components of droplet and gas velocities (R_{dg}) was obtained for the droplet size class '*D*' as a function of radius of separation (*r*). For the axial velocity, it is represented as $R_{ud*ug}(D, r)$ and is given as:

$$R_{ud*ug}(D,r) = \frac{\overline{\sum_{I}\sum_{J}\sum_{K} u_{d,I,J}(D) \times u_{g,I,K}(r)}}{u_{dr} \times u_{gr}} \qquad (1)$$

where u_{dr} and u_{gr} are the rms of the fluctuating component of velocity of droplet (with size class *D*) and gas in axial direction respectively and, u_d and u_g are the respective fluctuating components of velocity. *I* denotes any image sample while, *J* and *K* denote, respectively, the position of any droplet and, the surrounding gas velocities around the droplet and in an annular area defined within $r \pm \Delta r/2$. Similarly, the correlation coefficients for other combinations of velocity components are defined. Also, the spatial droplet-droplet velocity correlation, R_{dd}, was calculated in a similar fashion. Details about the choice of discrete values of *r* and Δr depending on droplet size class can be found in [14].

The plots of droplet-gas velocity correlations for axial and cross-stream velocity components, represented as R_{ud*ug} and R_{vd*vg} respectively, as a function of radius of separation, *r*, are shown in Fig. 4a and Fig. 4b respectively for different droplet size classes and also for three different cross-stream location. The statistical uncertainty of the correlation coefficient for 95% confidence interval is also shown for *R* = 0mm. The uncertainty of the correlation coefficients was low and of the order of ±0.002 for all droplet size classes. Considering the case of *R* = 0mm, Fig. 4a shows that the spatial correlation between the axial velocity fluctuations of droplets of all size classes and gas flow is quite high and decreases with distance away from the droplets (at larger *r*) though the change is quite low (~ 10%). This was somewhat expected. Since the particle stokes number was very small (*St* << 1), hence, the droplets of all three size classes can be expected to closely follow the gas motion and the flow can be considered to behave according to one-way coupling between the two phases within the experimental regime reported here. Also, comparing the value of R_{ud*ug} for the three size classes, no significant difference (< 0.1) in the correlation coefficient could be observed at any *r*. Thus, R_{ud*ug} can be considered to be independent of droplet size. However, in cross-stream direction, the magnitude of the droplet-gas velocity spatial correlation (R_{vd*vg}) was relatively lower and decreased fast with distance from the droplets as shown in Fig. 4b. Also, the magnitude of the correlation was relatively higher for the smallest droplet size class. Away from the spray axis (for *R* = 100 and 185mm), the axial correlation, R_{ud*ug} , increases though slightly for droplets of all size classes. However, a significant drop in cross-stream correlation, R_{vd*vg}, for all droplet sizes can be observed for the farthest measurement location, at *R* = 185mm. This is possibly because of the reduction in turbulence intensity in the cross-stream direction, as evident from the drastic drop (about 50%) in rms velocity in the same direction away from the spray axis.

In order to further elucidate the momentum transfer between the two phases, the normalized spatial correlation for the gas flow (R_{gg}) was obtained, as mentioned before, and compared with spatial correlations between droplet-droplet (R_{dd}) and droplet-gas (R_{dg}) velocity fluctuations. The spatial correlation of the axial gas velocity along the axial direction (R_{ug*ug}) and of cross-stream velocity in cross-stream direction (R_{vg*vg}) was calculated. Fig. 4c shows the comparison of the correlations for both velocity components for droplet size class 20-35 µm, at the three measurement locations, namely *R* = 0, 100 and 185mm. It can be observed that, at *R* = 0 and 100mm, both dispersed and continuous phases are well correlated with each other and also with themselves in this flow region, though the correlation is relatively higher in the axial direction. Though, all correlations have a slightly increasing tendency towards *R* = 100mm, which corresponds to the region of maximum turbulent shear stress.

For smaller radius of separation r or closer to the droplet, the value of the droplet-droplet correlation was slightly higher than the gas correlation because of the higher inertia of droplets as compared to gas elements. Away from the droplet, the correlation of droplet motion with the surrounding gas and also with other droplets (of same size class) tends to decrease, especially in the cross-stream direction. This effect is more pronounced for droplet sizes with higher relaxation time. However, the gas remains well correlated with itself even at large r, and thus for large r, along the cross-stream direction, $R_{gg} > R_{dd}$ and R_{dg}. At R = 185mm, considerable drop in droplet-droplet and droplet-gas correlations can be observed in cross-stream direction, which is, as explained before, because of the reduction in turbulent intensity in that direction. However, the gas correlation remains higher.

Influence of large scale flow structures on spatial correlation of droplet-gas velocity

In the study of droplet-laden two phase flow, it remains important and interesting to investigate the interaction between the dispersed phase and the large scale motions present in the continuous phase. But, this necessitates eduction of the large scale eddies from the instantaneous gas flow field surrounding the droplets. Out of several existing structure eduction methodologies, Proper Orthogonal Decomposition (POD), proposed by [16], provides an unbiased method to extract the large scale structures of a turbulent flow. POD essentially extracts a complete set of spatial eigen-functions or modes (also referred as the 'characteristic eddies of turbulence') from the measured two point velocity cross-correlation matrix. Thus, the shape of the extracted modes depends on the particular flow field and serves as a set of optimal basis functions for expansion of the flow. The velocity field can be represented as a sum of the modes. Also, because of the fastest convergence property, the number of energetically significant modes is minimum. In the present work, the POD modes of the turbulent gas flow are obtained using the 'method of snapshots', the details of which can be found in [17]. The details of the procedure can be found in [14]. Here only the results are presented.

In the present work, POD was applied over the instantaneous gas velocity data (for both axial and cross-stream velocity components) of the two phase spray measurements, after subtracting the mean velocity. Fig. 5a presents the flow structures associated with the 1st, 2nd and 3rd eigen-modes respectively at the measurement locations R = 0, 100 and 185mm respectively. The cumulative contributions of the eigen values of the POD modes are shown in Fig. 5b. For all cases, the contribution of the 1st eigen-value decreases away from the spray axis. This is attributed to the decreasing trend of the turbulent intensity towards outer spray. The 1st eigen mode contributes about 30% of the total turbulent kinetic energy and thus, it is the dominant eddy structure present in the continuous phase at all locations considered here. In total about 10 and 600 modes are required to represent 50% and 90% of the total kinetic energy respectively signifying very little contributions from the higher modes. Comparing the change in direction of the flow structures corresponding to the 1st mode for all three locations, the 1st mode can be expected to be a part of the largest eddies present in the gas phase flow with length scale of the order of 100mm. This is close to the estimated value of the largest length scale of the flow that was described earlier. The first eigen-mode indicates that the effect of these large scale structures (being mostly axial and upward/downward, Fig. 5a) is to either increase or decrease the instantaneous axial velocity of the gas flow, since the mean gas velocity is axial and either upward or downward (Fig. 3c). Similarly, the flow structure corresponding to the 2nd mode tends to increase/decrease the instantaneous cross-stream velocity towards/away from the spray axis. The 3rd mode in all cases shows the presence of a vortical structure spanning the whole measurement area. The decrease in length scales for higher modes can be observed.

It is important to investigate how each individual flow structure contributes towards the correlation between the dispersed and continuous phases present in the flow. For this purpose, for a given eigen-mode, the instantaneous velocity data were reconstructed by considering that mode only. Then, the spatial correlations of droplet-gas velocity fluctuations were calculated following the same procedure, as described in the previous section. Thus, the correlation is calculated for each mode conditional on each droplet size classes. Figures 6a and 6b show the modal contributions towards the droplet-gas velocity correlation for the droplet size class 20-35μm for axial and cross-stream velocity components respectively, at R = 0 mm. In the axial direction, the flow structure represented by the 1st mode produced maximum correlation value (~ 0.9) and found to be independent of the radius of separation. The 2nd mode showed low correlation, of the order of 0.1, and maintained the same value at any distance from a given droplet. The vortical structure, depicted by the 3rd mode, resulted in correlation, which was relatively high and positive closer to any given droplet but was negative away from it. The 4th and 5th modes, containing smaller vertical structures (not shown here), showed similar behavior, while, the other higher modes (after 10th mode), which may be characterized as random fluctuating components, showed very low correlation (~ 0.05). In contrast to the results in the axial direction, for cross-stream direction, the 2nd mode was dominant instead of the 1st mode. This was somewhat expected. The 2nd mode, being always dominant in cross-stream direction, correlated well with the droplet velocity in the same direction. Other modes produced a correlation, which is similar to the case of axial velocity component. For other larger droplet size classes, the contributions of modes to the droplet-gas velocity correlation, was similar to that of 20-35μm size class.

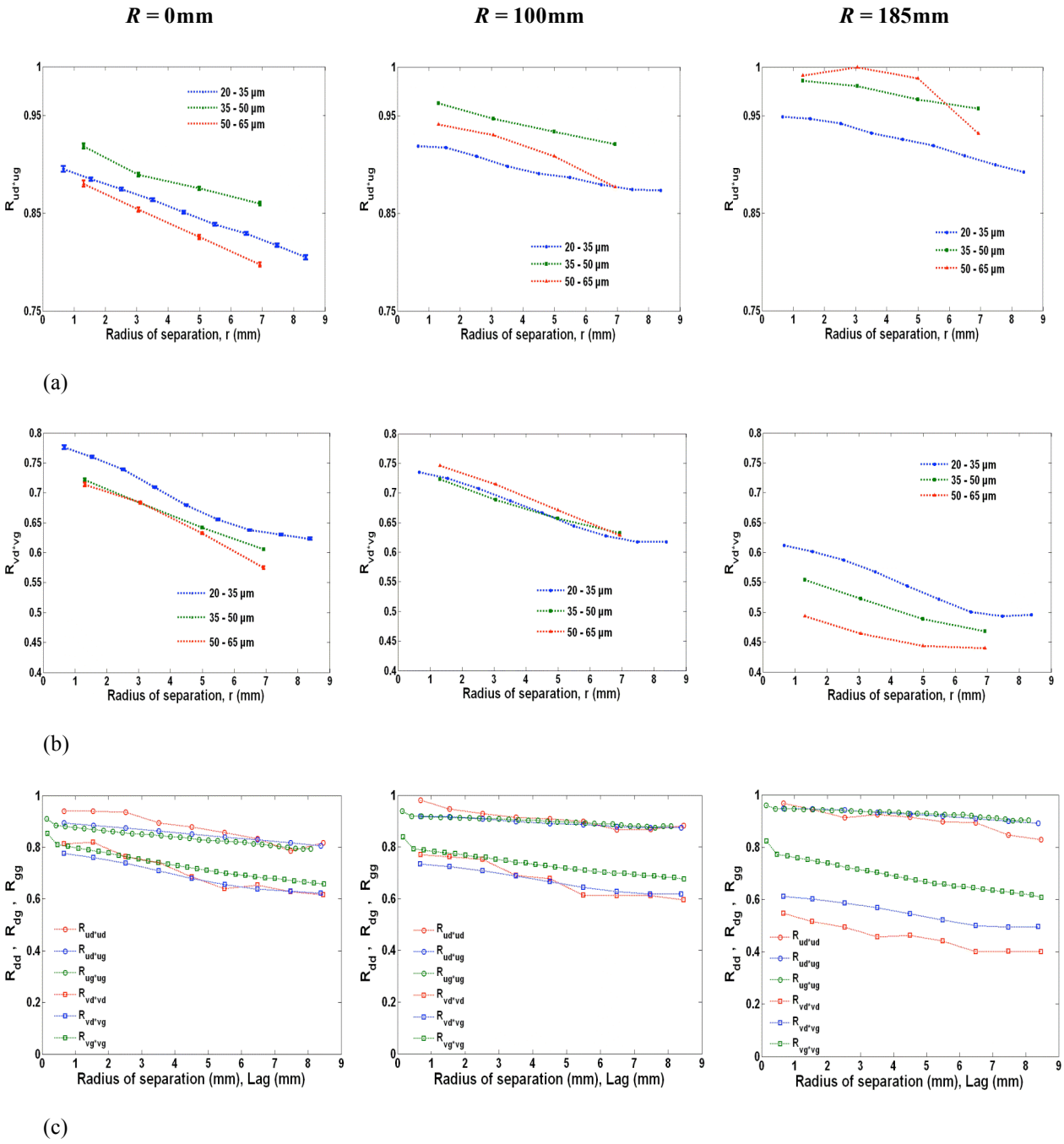

Figure 4: Spatial correlation coefficients of droplet-gas velocity fluctuations for the three droplet size classes for (a) axial component of velocity and (b) cross-stream velocity component, at R = 0, 100 and 185mm. Error bars for R = 0mm case indicate the statistical uncertainty of the correlation coefficient for 95% confidence interval. (c) Comparison of spatial correlation coefficients of droplet-droplet (R_{dd}) and droplet-gas (R_{dg}) velocity fluctuations for droplet size class 20-35µm and gas velocity correlation (R_{gg}) for both axial and cross-stream velocity components at the above mentioned cross-stream measurement locations.

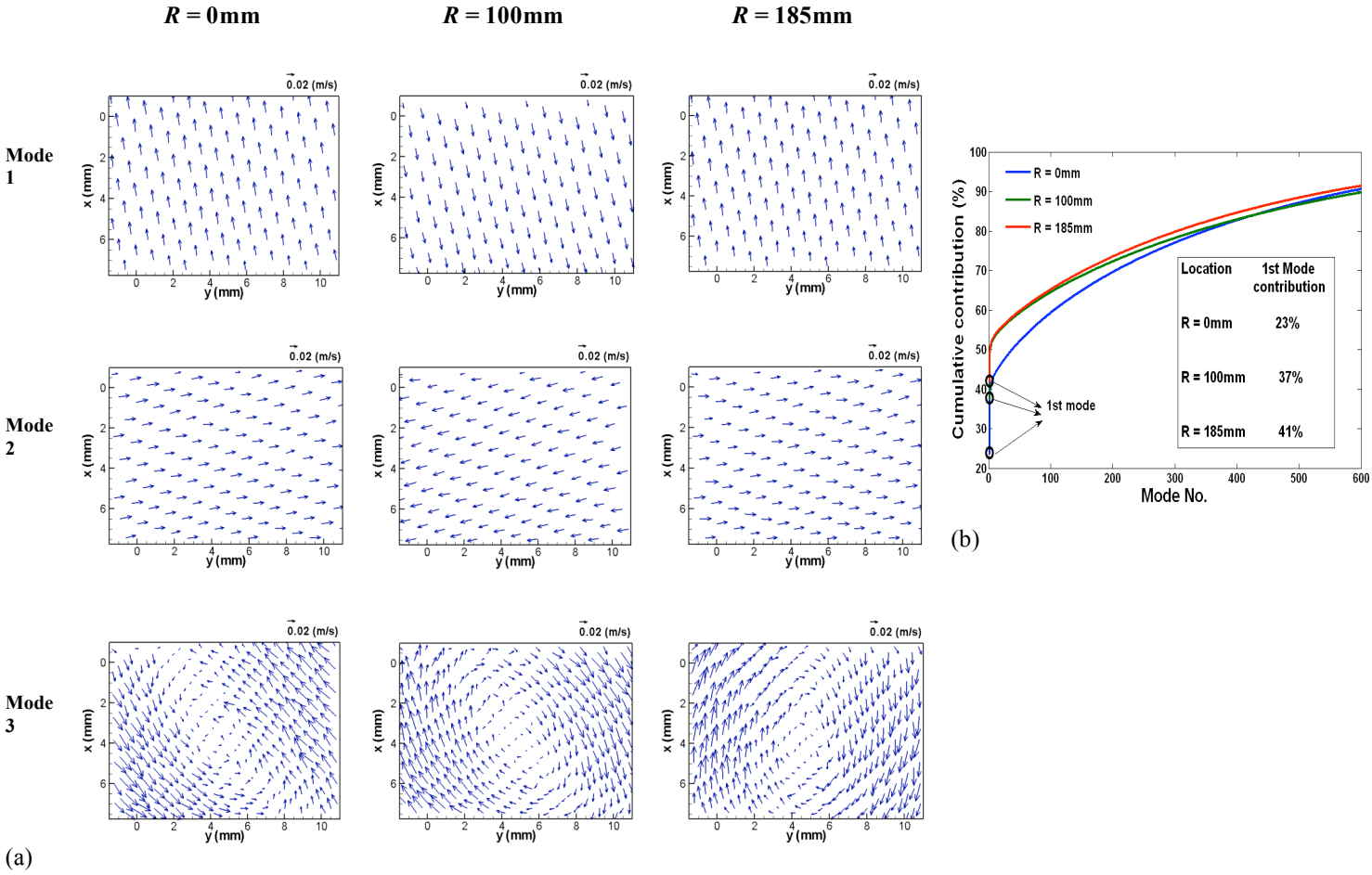

Figure 5: (a) Flow structures associated with 1st, 2nd and 3rd POD modes for the cross-stream measurement locations R = 0mm, 100mm and 185mm respectively (b) Cumulative contributions of the eigen-values of the respective POD modes for the three measurement locations. The contribution of the 1st mode for the three cases has been mentioned.

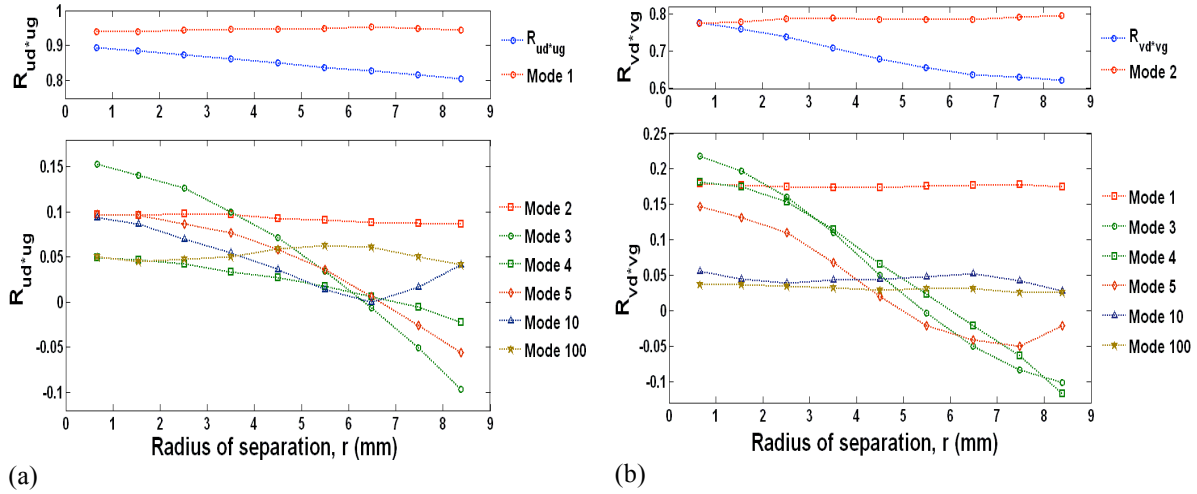

Figure 6: Contributions of various POD modes to the spatial correlation of droplet-gas velocity fluctuations for droplet size class 20-35µm at the measurement location R = 0 mm for (a) axial velocity component (R_{ud*ug}) and (b) cross-stream velocity component (R_{vd*vg}).

Combined ILIDS and LIF measurements

In this section, the combined ILIDS and LIF technique is demonstrated for a mono-sized droplet-stream. Two different droplet sizes were considered. Experiments were performed with a custom-built droplet generator, producing a single stream of mono-sized droplets. The injection pressure was set at 1.0 bar. The pinhole sizes at the exit of the mono-dispersed droplet generator were 200µm and 50µm respectively, while the corresponding water flow rate was 10.5 ml/min and 0.8 ml/min respectively. The resonance frequency of the piezoelectric elements of the generator was set to 20 kHz. Under this condition, the diameters of the droplets were approximately 252µm and 108µm respectively with an accuracy of 97% [18]. Figure 7 shows one of the instantaneous ILIDS and LIF images of the droplet stream, simultaneously obtained with the optical set-up described in section 2. The droplet size estimated by ILIDS was 268µm and 122µm respectively which are within 10% of the theoretically calculated values. Each droplet can be observed as a set of horizontal stripes of light in the ILIDS image in Fig. 7a. The fluorescence from both the droplet and its vapour appear on the LIF image. The large density difference between the liquid and vapour phases causes the fluorescence signal from droplets to be significantly higher than that of its vapour (the counts being of the order of about 1500:10) and thus, it is not possible to visualize both signals at the same time for a given dynamic range of the camera. Also, the halation of the droplet surrounding the droplet surface makes it difficult to discriminate the signals of the two phases. Hence the LIF images for both droplet sizes are shown here for two different dynamic ranges. For higher dynamic range, only the fluorescence from the liquid droplet and its halation can be observed in Fig 7b. The presence of fluorescence from the vapour can be seen in the lower dynamic range in Fig. 7c, while the liquid signal and its halation seem to be almost saturated. The inter-droplet distance was found to increase with smaller droplet size. Because of the closer spacing between the larger droplets, the vapour distribution was almost surrounding the whole droplet stream. For the droplet stream with smaller droplets, larger inter droplet spacing caused the vapour distribution of any two adjacent droplets to be quite discrete and mainly surrounding individual droplets. Because of interaction with the entrained air, the instantaneous vapour envelope around the whole stream of large droplet sizes was not symmetrical around the droplet stream, as expected.

Figure 8 presents the flow chart of the procedure used to obtain measurements of instantaneous droplet size, velocity and vapour distribution around the droplets from simultaneously recorded individual pairs of ILIDS and LIF images in a spray. The ILIDS images are first processed to obtain droplet size, velocity and position of the fringe patterns. The LIF images are processed to identify the droplet centres of the liquid fluorescence, which correspond to the image of the droplet centres in the object plane. After quantifying the droplet centre discrepancy using the mono-sized droplet stream for various positions in the object plane (laser sheet), the error is subtracted from the position of the centre of the fringe patterns in the ILIDS images obtained from the spray. For each fringe pattern in the ILIDS image, the corresponding vapour distribution is observed in the LIF image. Contributions from the liquid fluorescence and the droplet halation are filtered from the LIF images and, the images are processed to obtain the vapour concentration from the fluorescent intensity counts, using the calibration curve, as explained in section 2. Thus, the vapour distribution from individual droplets could be associated with the corresponding droplet size and velocity.

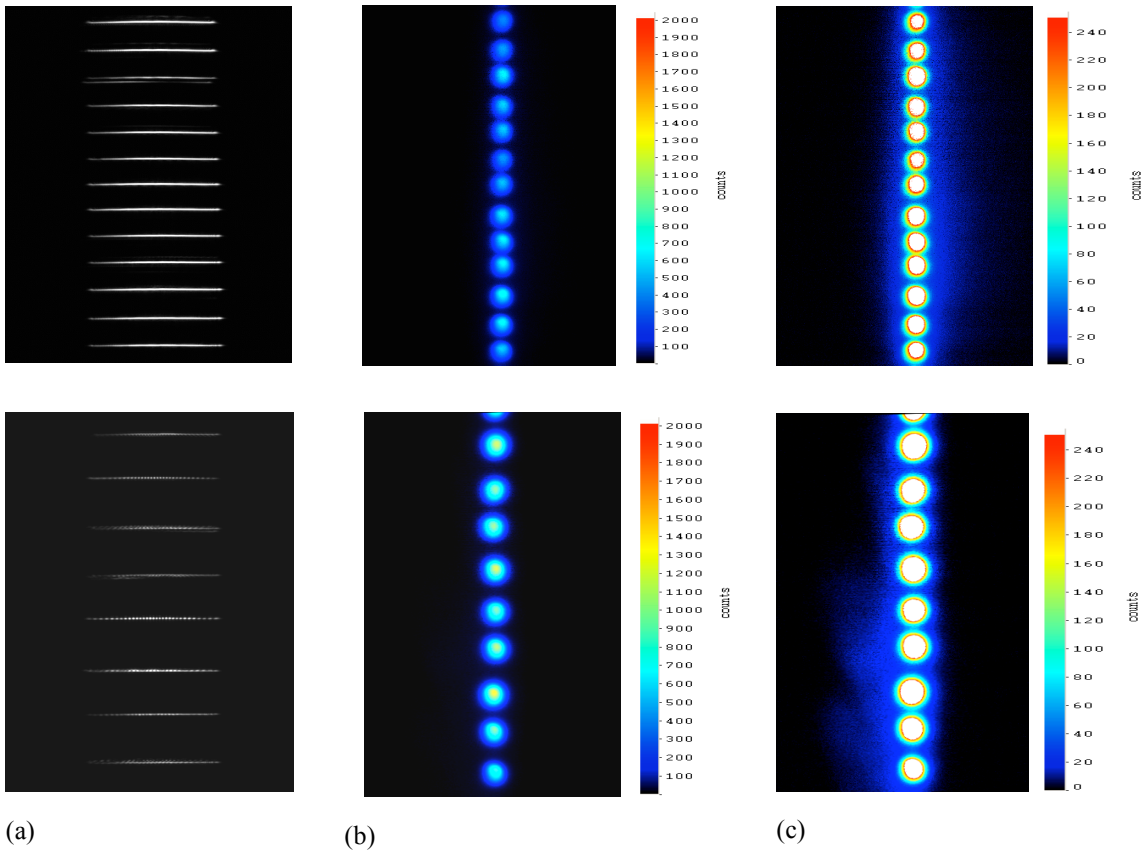

Figure 7: Simultaneous ILIDS and LIF images for mono-sized droplet stream of droplet sizes 268μm (top row) and 122μm (bottom row) respectively. (a) ILIDS images; (b) LIF images, shown with higher dynamic range; (c) The same LIF images, shown with lower dynamic range.

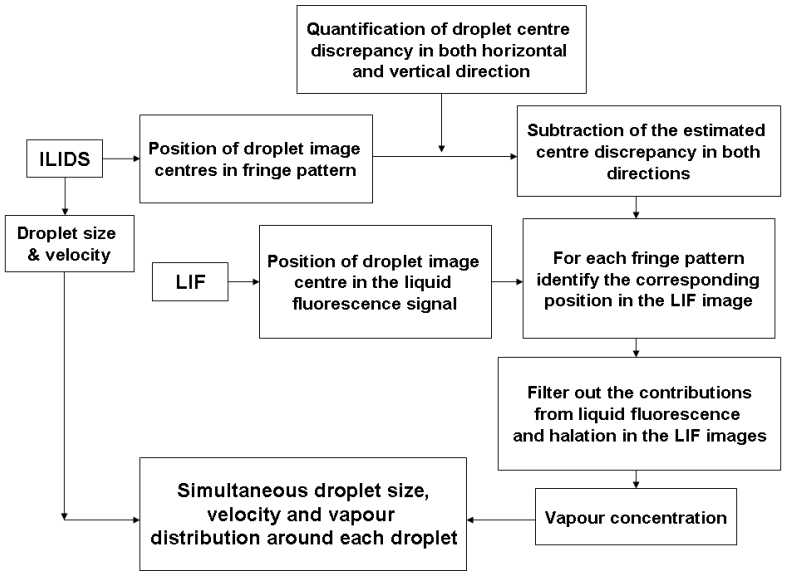

Figure 8: Flow chart for the measurements of instantaneous droplet size and velocity and, vapour concentration from simultaneously recorded individual pairs of ILIDS and LIF images.

Summary

Two novel approaches for simultaneous characterization of droplet and gaseous phases in isothermal and evaporative sprays were described. Both approaches use the out-of-focus imaging ILIDS technique for planar measurements of droplet size and velocity. The in-focus imaging techniques PIV and LIF are respectively com-

bined with ILIDS for simultaneous measurement of gas flow characteristics in an isothermal spray and vapour concentration measurement in an evaporative spray.

For the isothermal spray, combined ILIDS and PIV measurements are presented in a model co-flowing isothermal spray dryer corresponding to an off-axis plane, far downstream from the nozzle exit and consist of five different cross-stream locations at R = 0, 50, 100, 150 and 185mm respectively from the nozzle axis. At any *cross-stream location*, the mean droplet velocity was found to be low and independent of droplet size. The magnitude of the mean gas flow was found to be similar to that of the mean droplet flow. This could be explained by the behaviour of the entrained air flow, surrounding the spray in a recirculating pattern. The rms of velocity fluctuations of the droplet and gas phase flow were spatially homogeneous. The rms velocities of both phases were an order of magnitude greater than that of the mean. The spatial correlations of droplet-gas velocity fluctuations (conditional on droplet size classes) were determined as a function of the distance of separation between the droplets and gas or other droplets for both velocity components and for various cross-stream measurement locations. A relatively strong correlation between the axial components of droplet and gas velocities at every measurement location was observed, as compared to the cross-stream velocity component suggesting that the droplets faithfully follow the gas motion. This conclusion is expected from the low values of the turbulent Stokes number of droplets ($St << 1$) for the measurement location considered in the present work. Comparison of spatial correlation of the droplet-gas velocity fluctuations with the spatial correlations of droplet-droplet and gas velocity fluctuations was also presented. Along the distance R from nozzle axis and towards the outer spray, the droplet-gas spatial correlation had a tendency to increase in axial direction, and decrease in cross-stream direction. The large scale eddy structures were extracted by applying POD over the instantaneous gas velocity data. Contribution of individual POD modes on the droplet-gas spatial correlation was determined. At R = 0mm, the 1st mode for the axial velocity direction, and the 2nd mode, for the cross-stream velocity direction, were found to be the dominant contributors and the associated flow structures were identified. These results could improve the understanding of the interaction between the dispersed and continuous phases in a spray and, also could further elucidate the capability of the combined technique for two-phase spray measurements.

The optical arrangement for combined ILIDS and LIF techniques for simultaneous measurement of droplet size, velocity and vapour concentration in an evaporative spray was presented. The discrepancy in droplet centre due to the defocusing of the ILIDS technique was theoretically predicted. The droplet centre discrepancy was found to be varying approximately linearly across the image along the direction corresponding to the direction of propagation of the laser sheet for a given defocus setting in ILIDS. This result was similar to the combined ILIDS and PIV arrangement. The combined ILIDS/LIF technique was demonstrated for a mono-sized droplet stream for two droplet sizes of 268μm and 122μm respectively. The LIF images showed that the smaller inter droplet spacing of the larger droplet sizes, causes the vapour to surround the droplet stream. For smaller droplet sizes, the large droplet spacing allowed interaction of the vapour field with the surrounding air modifying the vapour distribution.

References

[1] Zimmer L., Domann R., Hardalupas Y. and Ikeda Y, *AIAA Journal,* 41:2170-2178 (2003).
[2] H.H.Chiu, T.M.Liu, *Combustion.Sci.Tech.* 17:127-142 (1977).
[3] Kulick, J. D., Fessler, J. R. and Eaton, J. K., *J. Fluid Mech.* 277: 109-134 (1994).
[4] Hardalupas Y, Horender S., Atomization Spray 13:273–295 (2003).
[5] Sakakibara, J., Wicker, R.B., Eaton, J.K., *Int. J. Multiphase Flow* 22: 863–881 (1996).
[6] Prevost, F., Boree, J., Nuglish, H.J. and Charnay, G., *Int. J. Multiphase Flow* 22: 685–701 (1996).
[7] Ferrand V, Bazile R, Boree J, Charnay G., *Int. J. Multiphase Flow* 29:195–217 (2003).
[8] Glover AR, Skippon SM and Boyle RD., *Applied Optics* 34:8409–8421 (1995).
[9] Kawaguchi T, Akasaka Y and Maeda M., *Meas Sci Technol* 13: 308–316 (2002).
[10] Hardalupas Y, Sahu S, Taylor AMKP and Zarogoulidis K. *14th Int Symp on Applications of Laser Techniques to Fluid Mechanics*, Lisbon, Portugal, 07-10 July (2008).
[11] Hardalupas Y, Sahu S, Taylor AMKP and Zarogoulidis K. *Experiments in Fluids* online (2010)
[12] Kurosawa R, Hishida K, Maeda M, *11th international symposium on applications of laser techniques to fluid mechanics*, Lisbon, Portugal, 8–11 July(2002).
[13] Hardalupas Y, Sahu S, Taylor AMKP and Zarogoulidis K, *AIAA*-2009-0995. Florida, USA, (2009).
[14] Hardalupas Y, Sahu S, Taylor AMKP and Zarogoulidis K, *7th ICMF*, Florida, US, 30th May-4th June (2010).
[15] Tennekes H and Lumley J. L., *A First Course in Turbulence*. MIT press. Cambridge (1972).
[16] Lumley, J.L., *Coherent structures in turbulence.* Transition and Turbulence (1981)
[17] Sirovich, L., *Quart. J. Appl. Math*., 45:561–590 (1987)
[18] Pergamalis H, *PhD thesis*, Imperial College London (2002).